2017 25th Mediterranean Conference on Control and Automation (MED)
July 3-6, 2017. Valletta, Malta

On the detection of solar panels by image processing techniques*

Santiago Salamanca, Pilar Merchán, and Iván García.

Abstract— **This paper proposes a solution based on computer vision to detect solar panels in images. It is based on the definition of a feature vector that characterizes portions of images that can be acquired with a standard camera and with no lighting restrictions. The proposal has been applied to a set of images taken in an operating photovoltaic plant and the results obtained demonstrate its validity and robustness. These results are meant to be used in later stages of a procedure for the optimization of energy efficiency.**

I. Introduction

As known, solar energy is one of the most important and cleanest source of renewable energy available. There are several ways to harness solar energy, which can be roughly classified into passive or active. The main difference between them is whether they use or not mechanical or electrical devices to convert the sun's heat or light to another form of usable energy. Photovoltaics (PV) is an example of active systems. PV devices generate electricity directly from sunlight via the electronic process that occurs directly in semiconductors, known as photovoltaic effect.

A typical photovoltaic system employs solar panels that can be mounted either in a fixed position or on trackers that follow the sun across the sky. Nowadays, trackers are used in most of the operating installations to minimize the angle of incidence between the incoming sunlight and the photovoltaic panel. This increases the amount of energy produced from a fixed amount of installed power generating capacity.

There are two types of sun tracking systems [1]: closed-loop and open-loop systems. In closed-loop systems the orientation of the solar panel is controlled by using a feedback control system [2]. The proposal of Wei et al. [3] uses image sensors to detect the brightest region in the sky and direct the photovoltaic panel perpendiculary to the sun in real-time. In the second type, open-loop systems, the orientation of the solar tracker is set by applying a solar position algorithm [4]. In this case, there is no way to determine whether the desired position is achieved or not. Errors in the orientation of the solar tracker can arise and they generate losses in the production of electrical energy. Fig. 1 shows the appearance of a solar plant in which most solar trackers are misdirected. Although closed-loop systems present benefits in sun tracking, nowadays most of the installed systems are open-loop solar trackers.

The energy efficiency of these plants can be influenced by a large variety of factors. Many of them are monitored using specific measuring devices, such as temperature sensors, irradiance sensors, current sensors, etc. However, there are other factors whose evaluation is not trivial, and the use of other methods is necessary. These factors are mainly related to faulty operation of the photovoltaic panels, such as the hot-spot effect or the appearance of shadows on the plates. In this field, especially the hot-spot detection, the working procedure using thermographic cameras is perfectly defined and can be employed in photovoltaic installations [5]. However, the detection process is carried out manually, so it is usually a slow and expensive procedure. Some works have recently been published that use drones to overcome this situation [6].

On the other hand, the orientation of the solar tracker is a fundamental aspect for the correct generation of energy by the solar trackers. This latter point is the ultimate goal of our research, that is focused on detecting and monitoring the orientation of the solar trackers in an operating solar plant, automatically and in real-time, to generate reports that can be used by the maintenance services of the plants. The work presented in this paper constitutes the initial stage.

Here, we propose a method to detect solar panels in images of operating photovoltaic plants taken with standard cameras and no special lighting conditions. Detection of stationary foreground objects has attracted the attention of many researchers over the last decades and, consequently, many new ideas have been recently proposed, trying to achieve high-quality detections in complex scenarios with the lowest misdetections, while keeping real-time constraints. Cuevas *et al.* [7] provide a complete survey of the most relevant approaches to detect all kind of stationary foreground objects. Our proposal is based on the definition of a feature vector that classifies the pixels of the image as belonging or not belonging to a solar panel. This vector is computed from the co-occurrence matrix [8, 9]. The co-occurrence matrix was proposed as a feature for the detection of textures in images. A photovoltaic plate, as can be seen, for example, in figure 4, can be considered like this. Statistical characteristics [10] are usually determined from the co-occurrence matrices for the detection of textures. However, in this work we propose a geometric characteristic measured on the co-occurrence matrix that is less time consuming than the previous ones. The experimental results prove that our proposal is suitable to detect solar panels in images and provide a starting point of a procedure to monitor solar trackers in order to optimize energy efficiency. To the

*This work has been supported by the FEDER Funds (Programa Operativo FEDER de Extremadura 2014-2020) through the grant "Ayuda a Grupos de Investigación" (ref. GR15178) of Junta de Extremadura, and by Gobierno de Extremadura and Fondo Social Europeo (ref. PCJ100402).

Santiago Salamanca is with the Escuela de Ingenierías Industriales, University of Extremadura, Avda. de Elvas s/n, 06006 Badajoz, Spain (phone: +34924289300; fax: +34924289601; e-mail: ssalamanca@unex.es).

Pilar Merchán is with the Escuela de Ingenierías Industriales, University of Extremadura, Avda. de Elvas s/n, 06006 Badajoz, Spain (e-mail: pmerchan@unex.es).

Iván García is with the Escuela de Ingenierías Industriales, University of Extremadura, Avda. de Elvas s/n, 06006 Badajoz, Spain (e-mail: ivan@unex.es).

978-1-5090-4533-4/17/$31.00 ©2017 IEEE

best of our knowledge, there are no previous works in this area.

The remainder of the paper is structured as follows. In section 2 the type of images used to detect the solar panels and the environmental conditions needed to take them are exposed. Section 3 is devoted to show the procedure proposed for the detection of solar panels. Section 4 shows the experimental results. At last, section 5 states the conclusions and future works.

II. IMAGE ACQUISITION

The images of the solar panels are taken with a standard camera and no special lighting conditions. In order to have a broader file of vision the camera is placed in a telescopic tripod. This tripod has a motorized Pan & Tilt head where the camera is mounted (Fig. 2), so that it is possible to control the position of the camera to acquire images of a greater number of panels. Fig. 3 shows the assembly of the tripod in the photovoltaic plant.

Fig. 4 offers an example of the kind of images that have been taken and analysed.

III. PANEL DETECTION

The detection of the panels is performed by applying a segmentation process that separates the surfaces of the photovoltaic panels from the surroundings in the images acquired.

The segmentation algorithm is based on the definition of the *feature vector*,υ, a characteristic that allows for the classification of the pixels as belonging or not belonging to a solar panel. Thus, the relevant data of the image are extracted and the rest disregarded.

A. Feature Vector Definition

As commented in the Introduction section, the *feature vector*,υ, is defined from the grey-level co-occurrence matrix, also known as the grey-level spatial dependence matrix. As known, it is a statistical method to examine texture that considers the spatial relationship between pixels. The grey-level co-occurrence matrix characterizes the texture of an image by calculating how often pairs of pixels with specific values and spatial relationships occur in an image.

To calculate these matrices, we begin by cutting several images into small windows of fixed size. These windows are taken from areas of the images that correspond to solar panels and areas that do not correspond to solar panels. After this, two co-occurrence matrices, denoted as M_{CO}, (taking into account horizontal or vertical neighbourhood between pixels) are determined for every extracted portion, with the purpose of identifying a pattern followed by the segments of interest, i.e., we want to find out the similarity between the co-occurrence matrices associated with areas belonging to the solar panels.

Figure 1. Aerial picture of a solar plant. Errors in the orientation of the solar trackers are noticeable (Source: Google Earth)

Figure 2. Motorized Pan &Tilt tripod head.

Figure 3. Telescopic tripod assembly in the photovoltaic plant.

Figure 4. Example of image taken by the camera mounted on the tripod.

If these matrices are represented as binary images, I_{CO}, scattered points as to the ones shown in Fig. 5 are obtained. As seen in the images, and after analysing the matrices of each segment, the scattered points belonging to pieces of panel surfaces (Fig. 5(a)) always present a comet shaped pattern. In the case of windows containing portions corresponding to no panels, these images have a different and more variable pattern (Fig. 5(b)). Let us consider this in more detail to discern if the use of the co-occurrence matrices as discriminating features for the areas of the image where there is panel surface is justified.

The reason for this comet shape could be understood if two questions are considered regarding the panel's portions, namely: their histograms and their topological relationships.

With respect to histograms, it is noticeable that in all of them two different zones can be identified. They both can be approximated to a normal distribution functions, with mean values μ_d and μ_l and standard deviations σ_d and σ_l. Each zone corresponds to pixels with darker (μ_d) or lighter (μ_l) grey level value, that is, $\mu_d < \mu_l$. On the other hand, in all cases, $\sigma_d < \sigma_l$ is verified. Fig. 6 shows an example: Fig. 6(a) is one of the portions of the original image and it is part of a panel surface; in Fig. 6(c) the normalized image histogram together with the two distribution functions are depicted, in black the one for the lighter zones and in red for the darker ones. Fig. 6(b) offers the same initial portion with a superimposed mask in which dark areas, formed by the pixels having an intensity values between μ_d-σ_d and μ_d+σ_d, are marked in red and the light zones, determined by the pixels with values between μ_l-σ_l and μ_l+σ_l are green.

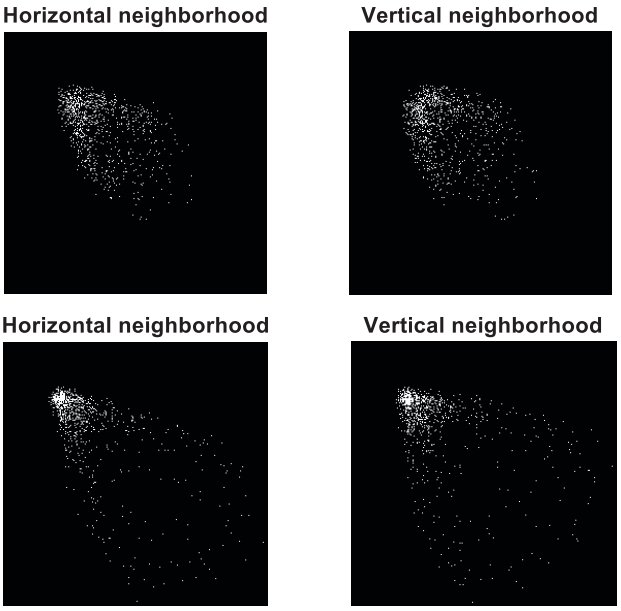

(a)

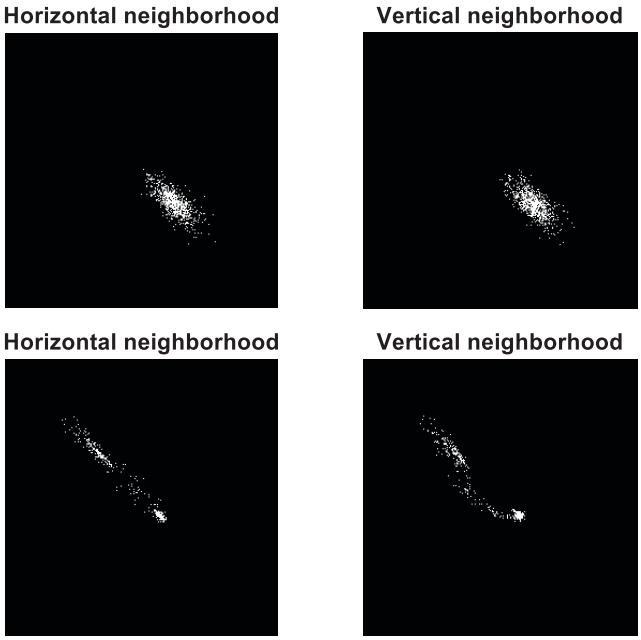

(b)

Figure 5. Co-occurrence matrices for portions of image corresponding to panel surfaces (a) and corresponding to the surroundings of solar panels (b).

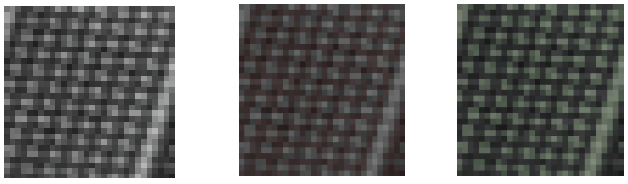

(a) (b)

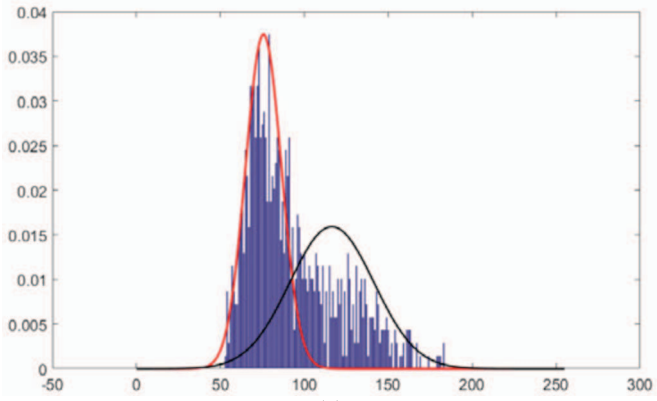

(c)

Figure 6. (a) Segment of the image belonging to a panel surface. (b) Dark and light areas segmented using the normal distributions depicted in (c). (c) Normalized histogram of the segment in (a) and approximated normal distributions.

With respect to topological relationships, taking into account the meaning of the co-occurrence matrix and since there exist two grey levels in I_{CO}, these relationships are of four different types. Assuming, for example, a horizontal neighbourhood relation, they will be:

- dark pixel ($\mu_d \pm \alpha \cdot \sigma_d$) which has on its right another dark pixel ($\mu_d \pm \alpha \cdot \sigma_d$);
- dark pixel ($\mu_d \pm \alpha \cdot \sigma_d$) which has on its right a ligth pixel ($\mu_l \pm \beta \cdot \sigma_l$);
- light pixel ($\mu_l \pm \beta \cdot \sigma_l$) which has on its right another ligth pixel ($\mu_l \pm \beta \cdot \sigma_l$) and
- light pixel ($\mu_l \pm \beta \cdot \sigma_l$) which has on its right a dark pixel ($\mu_d \pm \alpha \cdot \sigma_d$)

α and β being real numbers greater than 1.

These relationships define 4 zones, two circular zones having centres (μ_i, μ_i) and radii proportional to σ_i, and two ellipsoidal zones having centres (μ_i, μ_j) and semi-axis lengths σ_i and σ_j, where i and j correspond, indistinctly, to subscripts d and l. When they are represented on the image I_{CO}, the circular and ellipsoidal zones circumscribe, approximately, the scattered points (Fig. 7(a)). Fig. 7 (b) shows two more examples of this fact.

The images resulting from applying the same procedure to portions that do not correspond to panel surface are displayed in Fig.8. It can be seen, as mentioned in previous paragraphs, that in these cases neither the shape of the points nor the distribution of the light and dark zones correspond to the pattern detected in the portions of panels.

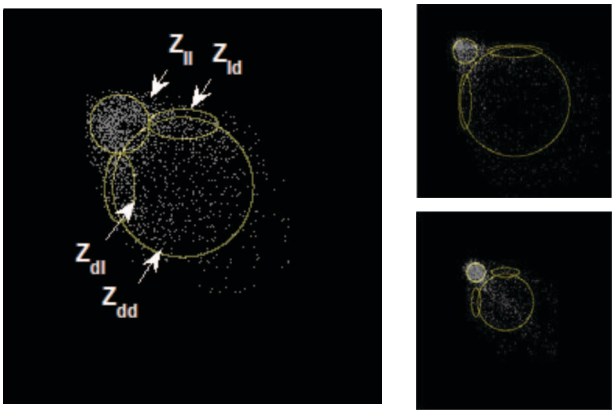

(a) (b)

Figure 7. Representation of the areas obtaiened from the definition of light and dark zones and the topological relationship, in a portion of the solar panel for α=β=1.8.

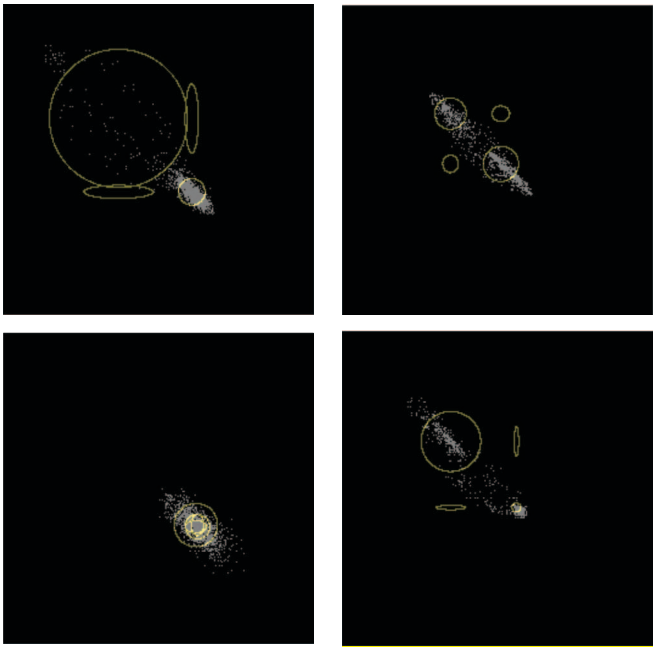

Figure 8. Co-occurrence matrices representations for portions that do not correspond to panel surface.

In an offline process, we generate a benchmark of patterns that serve as models for the segmentation. These patterns are created from a large number of different portions belonging to solar panels. Fig. 9 left shows some of the windows containing pieces of solar panel that have been used to define these patterns.

Afterwards, an OR-logic operation is performed between the two co-occurrence matrices in order to retain the information provided by both of them in a single image (*CM* hereafter). A reference system is defined for the concentration of points of each *CM* by determining its principal components [11]. The first component corresponds to the axis where the distance between the ends of the coordinate projections is maximum. The second principal component defines an orthonormal axis to the first one. The coordinate origin coincides with the concentration of points' centre of mass. Following, the principal axis is divided into several equal segments and two parameters are calculated for each generated part: the total number of points inside the part, and the maximum distance between the two more distant points to the principal axis (see Fig. 9 right).

After the aforementioned calculations, two vectors, N_j and D_j, are defined as

$$N_j = \bigcup_i \frac{1}{\max\{n_1^i, n_2^i, \ldots, n_j^i, \ldots, n_m^i\}} n_j^i \quad (1)$$

$$D_j = \bigcup_i d_j^i \quad (2)$$

Where j=1, …, m is the number of parts, i is the i-th pattern, n_j^i stores the number of points of the j-th part in the i-th pattern, and d_j^i is the maximum distance between the more distant points of the j-th part in the i-th pattern.

Finally, N_j and D_j are approximated to a normal distribution function [12] characterized by its media, μ_j, and its standard deviation, σ_j. These are the values that make up the *feature vector*, υ:

$$\upsilon = \begin{Bmatrix} \mu_1^N, \sigma_1^N, \mu_1^D, \sigma_1^D \\ \mu_2^N, \sigma_2^N, \mu_2^D, \sigma_2^D \\ \vdots \\ \mu_j^N, \sigma_j^N, \mu_j^D, \sigma_j^D \\ \vdots \\ \mu_m^N, \sigma_m^N, \mu_m^D, \sigma_m^D \end{Bmatrix} \quad (3)$$

B. Segmentation Stage

Once the patterns for panel have been defined the segmentation phase can be undertaken. The algorithm designed to segment can be described roughly as follows: first, the image to be analysed is divided into portions; secondly, the *feature vector* υ is calculated for each of the portions, thirdly, the vector probability of belonging to the panel class is calculated. Let us now consider the algorithm details.

To begin with, the image under study is traversed portion by portion. These portions or fragments, *F*, are defined with the same size as the ones used in the phase of pattern definition.

For each fragment *F*, the co-occurrence matrix is calculated and vectors $N^F=\{n_1^F, n_2^F,..., n_j^F,..., n_m^F\}$ and $D^F=\{d_1^F, d_2^F,..., d_j^F,..., d_m^F\}$ are obtained, as explained in section III.A.

Then, the probability of being part of the distributions defined in the row *j* of vector υ (given by μ_j^X and σ_j^X) are determined for every vector value, n_j^F and d_j^F, by using the expression:

$$p_j^X = P\left(x_j^F \middle| \mu_j^X, \sigma_j^X\right) = \frac{1}{\sigma_j^X\sqrt{2\pi}} \int_{-\infty}^{n_j^N} e^{\frac{-\left(t-\mu_j^X\right)^2}{2\left(\sigma_j^X\right)^2}} dt \quad (4)$$

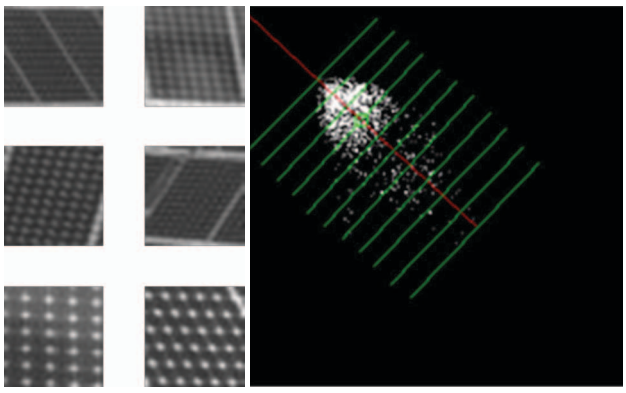

Figure 9. Left: Fragments used in the offline stage for the determination of feature vector υ of patterns. Right: CM of a particular portion with its principal axis depicted in red and the lines that define the several parts in green.

Where *X* refers to either *N* or *D* depending on whether the probability is calculated for the number of points or the maximum distance in each partition. Initially, we assume that both probabilities are independent and, therefore, the joint probability is determined as

$$p_j^F = P\left(n_j^F, d_j^F\right) = p_j^N \cdot p_j^D \quad (5)$$

Finally, the average value of all probabilities is obtained by means of

$$\overline{p^F} = \frac{1}{m}\sum_{j=1}^{m} p_j^F \quad (6)$$

This value determined in (6) is used to decide whether the pixels that form *F* are marked as belonging to the panel class or not. If we denote this class as $C_{i,j}$ for the pixel $(i, j) \in F$ and give it the value 1 if the pixel corresponds to a panel pixel and 0 otherwise, the assignment function for $C_{i,j}$ is defined as follows:

$$C_{i,j} = \begin{cases} 1 \; if \; \overline{p^F} \geq \lambda \\ 0 \text{ otherwise} \end{cases} \quad (7)$$

Where λ is a threshold value.

IV. Results

We have applied our method to a set of images taken in an operating photovoltaic plant. They are grey-scale images in JPG format and their resolution is 753x566 pixels. The camera was placed in a telescopic tripod that can reach 12 meters high and includes brackets that allow its anchoring to the floor.

The algorithms were programmed in Matlab. Regarding these algorithms, there are several aspects to be pointed out:

- The fragments of image belonging to solar panel used to determine the *feature vector* in the offline process were 30x30 pixels sized, and the *CM* image was computed for each one of them. A total of 100 fragments were used to define the patterns, some of them were shown in Fig. 9. Left.
- As mentioned in section II, *CM* image was calculated from the following co-occurrence matrices:
  - Horizontal co-occurrence matrix: the nearby pixel is located just to the right of the reference pixel.
  - Vertical co-occurrence matrix: the nearby pixel is below the reference pixel.
- The principal axis was computed by identifying the principal components of the pixel coordinates for each *CM*. It has been divided into 10 segments; this value was adjusted by trial and error. As explained, N_j and D_j are calculated for the *j*-th part and, from them, the *feature vector*, υ. Fig. 10 is made up of two graphs illustrating the mean values, μ, and the deviation, σ, represented the latter with an error bar, for the number of normalized data (a) and the maximum distance between points (b).
- The threshold value was set to λ=0.5.

Finally, the results achieved after applying the procedure explained in section III in several images are shown in Fig.

11. The regions identified as solar panel are depicted in green, and the areas labelled as not belonging to solar panel are depicted in red. As seen, there are hardly any false positives. However, the number of false negatives is greater, mainly related to changes in image scale.

V. Conclusion

This paper offers a procedure based on computer vision for the detection of solar panels in images taken in operating photovoltaic plants that can be acquired with a standard camera and with no lighting restrictions. It is based on the calculation of the co-occurrence matrices for fragments of images. We have proved that matrices corresponding to fragments of solar panels produce a black and white representation that resembles the shape of a comet. Taking advantage of the peculiarity of these images, two measures that allow to calculate the probability that a fragment is part of a panel or not have been proposed on them. The application of this method does not require any prior image processing procedure.

The proposal has been applied to a set of images taken in natural environments and the results so far are promising and demonstrate that the method can be used for the intended purpose.

As future work, we aim to adapt the method so that the results are valid at different scales and thus the number of false negatives is reduced.

References

[1] C.Y. Lee , P.C. Chou, C.M. Chiang, and C.F. Lin, "Sun tracking systems: a review," *Sensors (Basel)*, vol. 9, no. 5, pp. 3875–3890, May 2009.

[2] M. Berenguel, F.R. Rubio, D. Martínez, and E.F. Camacho, *Control of solar energy systems*. Springer, 2012, pp. 53–65.

[3] C. Wei, Y. Song, C. Chang and C. Lin, "Design of a Solar Tracking System Using the Brightest Region in the Sky Image Sensor", *Sensors* 16(12), pii: E1995, 2016.

[4] I. Reda, and A. Andreas, "Solar position algorithm for solar radiation applications," *Sol. Energy*, vol. 76, no. 5, pp. 577–589, 2004.

[5] M. Simon and E. Meyer, "Detection and analysis of hot-spot formation in solar cells", *Solar Energy Materials and Solar Cells*, vol. 94, no. 2, pp. 106–113, 2010.

[6] J. Tsanakas, L. Ha, and F. Al Shakarchi, "Advanced inspection of photovoltaic installations by aerial triangulation and terrestrial georeferencing of thermal/visual imagery", *Renewable Energy*, vol. 102, part A, pp. 224–233, March 2017.

[7] C. Cuevas, R. Martinez, N. García, "Detection of stationary foreground objects: A survey". *Computer Vision and Image Understanding*, 152, 41–57, 2016.

[8] R.M. Haralick, K. Shanmugam, I. Dinstein "Textural Features for Image Classification", *IEEE Transactions on Systems, Man, and Cybernetics*, vol. SMC-3, no. 6, pp. 610–621, Nov. 1973.

[9] R.C. Gonzalez, R.E. Woods, *Digital Image Processing (3rd Edition)*. Pearson Prentice-Hall, Inc., pp. 822–839, 2008.

[10] J. Tou, Y. Tay, and P. ,Lau, "One-dimensional Grey-level Co-occurrence Matrices for texture classification," in *Proc. of International Symposium on Information Technology*, Kuala Lumpur, pp. 1–6, 2008.

[11] J. Shlens, "A Tutorial on Principal Component Analysis". arXiv:1404.1100, Apr. 2014.

[12] J.A. Rice Mathematical Statistics and Data Analysis (Third Edition). Thomson, 2007.

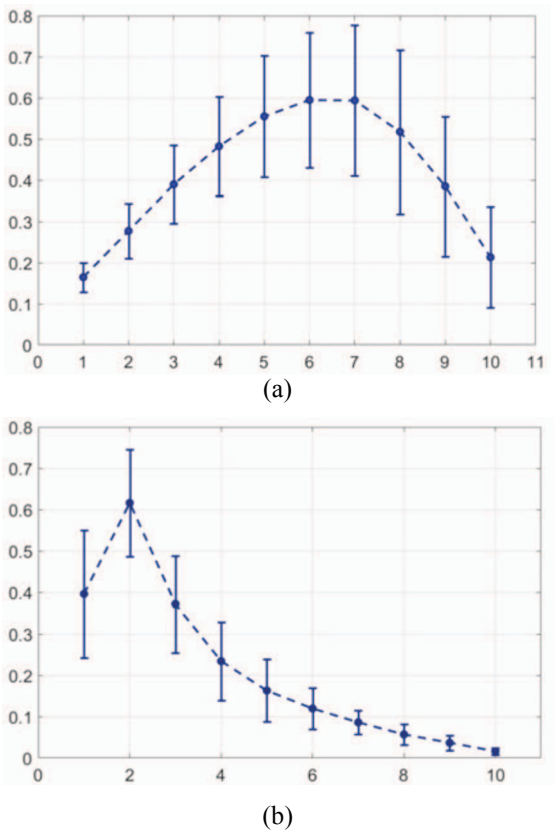

Figure 10. Representation of μ and σ for (a) the number of normalized data and (b) the maximum distance between points.

Figure 11.

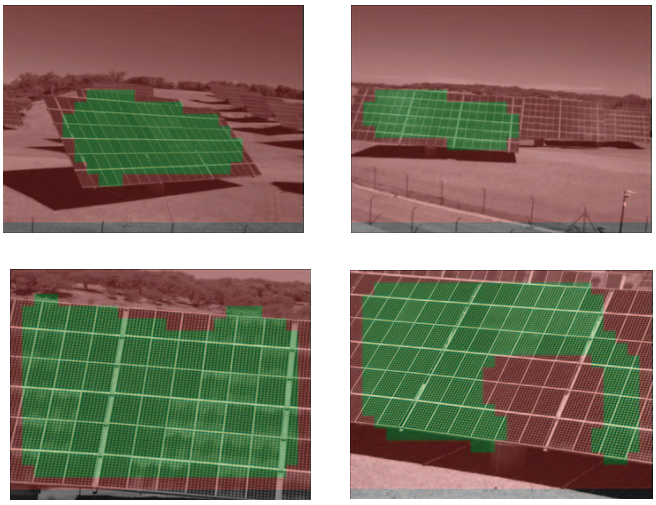

Figure 12. Segmentation results. The zones identify as panel are depicted in green and the areas catalogued as no panel in red.